JPE 19-2-12

https://doi.org/10.6113/JPE.2019.19.2.463
ISSN(Print): 1598-2092 / ISSN(Online): 2093-4718

Effect of Winding Configuration on the kVA Rating of Wye-connected Autotransformer Applied to 12- pulse Rectifier

Fangang Meng†, Qingxiao Du*, Lei Gao*, Quanhui Li*, and Zhongcheng Man*

†,*School of Electrical Engineering, Harbin Institute of Technology, Harbin, China

Abstract

This paper presents the effect of winding configuration on the kVA rating of a wye-connected autotransformer applied to a 12-pulse rectifier. To describe the winding configuration of the wye-connected autotransformer, position and proportional parameters are defined and their quantitative relation is calculated. The voltages across and currents through the windings are measured under different winding connections. Consequently, a relation between the kVA rating and position parameter is established in accordance with the analysis, and the optimal winding configuration is obtained on the basis of this relation. A wye-connected autotransformer with the least equivalent kVA rating and simplest winding configuration is designed and applied to the 12-pulse rectifier. Simulations and experiments are conducted to validate the theoretical analysis.

Key words: kVA rating, Optimal design, Winding configuration, Wye-connected autotransformer

I. INTRODUCTION

Multi-pulse rectifiers (MPRs) with low electromagnetic interference are widely used in high-power rectifications due to their superior performances in harmonic elimination at AC input and ripple reduction at DC output [1]-[3]. Generally, the MPR is composed of a phase-shifting transformer and two or more three-phase rectifiers [4]. The phase-shifting transformer is used to produce two or more sets of three-phase voltages and to feed the three-phase rectifiers. Moreover, the primary magnetic device in the MPR is the phase-shifting transformer, which determines the MPR volume. To improve the power density of the MPR, the volume of the phase-shifting transformer should be reduced [5]-[7]. In general, the volume of the phase-shifting transformer is determined by its kVA rating. Therefore, reducing the kVA rating of the phase-shifting transformer has become a popular topic in the design of MPRs.

The phase-shifting transformer is classified into two types, namely, isolated transformer and autotransformer [8], [9]. If the required output voltage is considerably higher or lower than the input voltage, then the isolated transformer is preferred in the viewpoint of protection. For example, in electroplating, the load voltage is only approximately 10 or more volts, which is considerably lower than the input voltages. In this application, the isolated transformer is preferred. The isolated transformer uses the magnetic coupling to transmit the load power; hence, the apparent power of the isolated transformer is equal to or more than the load power [10]. Therefore, if the isolated transformer is used as the phase-shifting transformer, then the MPR is bulky. If the required output voltage of the phase-shifting transformer is approximately equal to its input voltage, then the autotransformer is the best option as the phase-shifting transformer. As the windings of the autotransformer are interconnected, only a small fraction of the load power is transmitted by magnetic coupling [11]-[13]. Therefore, the apparent power of the autotransformer is less than the load power, thereby reducing the bulk of the phase-shifting transformer.

In MPRs, the autotransformer is classified into six, nine, 12, or more phases in accordance with the phase number. Among them, the six-phase autotransformer is frequently used because of its least kVA rating under the same load power. This

Manuscript received Oct. 30, 2018; accepted Dec. 14, 2018
Recommended for publication by Associate Editor Li Zhang.
†Corresponding Author: mfg0327@sina.com
Tel: +86-631-5687068, Harbin Institute of Technology
*School of Electrical Engineering, Harbin Institute of Technology, China

autotransformer includes delta-, wye-, and polygon-connected autotransformers. Although the autotransformers are often used for high-power rectification, not all arbitrarily configurated autotransformers can reduce the MPR bulk. In [11], Meng et al. analyzed the winding configuration on the kVA rating of a delta-connected autotransformer; they reported that the bulk can only be reduced when the autotransformer is optimally designed. In this study, we analyze the winding configuration on the kVA rating of the wye-connected autotransformer and provide an interesting and useful confirmation that the well-used circuit is optimal in terms of kVA rating. Finally, we provide an additional insight into these devices and how they may be analyzed.

II. Requirement of 12-Pulse Rectifier on the Wye-Connected Autotransformer

Fig. 1 shows a 12-pulse rectifier with a wye-connected autotransformer. In Fig. 1, an inter-phase reactor (IPR) is used to absorb the instantaneous difference of the output voltages and ensure the independent operation of the two bridge rectifiers [14]. A zero-sequence blocking transformer is utilized to promote a 120° conduction for each rectifier diode due to high impedance to zero sequence currents [14]. The main function of the wye-connected autotransformer in Fig. 1 is to produce two sets of three-phase voltages with appropriate phase-shift angles. As discussed in [15], to eliminate the (12k±1)th (k is an odd number) harmonics, the phase-shift angle should meet

$$2\alpha = \frac{60^\circ}{M}, \tag{1}$$

where M denotes the number of three-phase diode bridge rectifiers.

Therefore, the phase-shift angle between the sets of three-phase voltages should be 30°. Assume the input three-phase voltage of the wye-connected autotransformer as

$$\begin{cases} u_a = \sqrt{2}U_m \sin \omega t \\ u_b = \sqrt{2}U_m \sin(\omega t - 120^\circ) \\ u_c = \sqrt{2}U_m \sin(\omega t + 120^\circ), \end{cases} \tag{2}$$

where U_m is the amplitude of the three-phase input voltage.

From Eqs. (1) and (2), the two sets of three-phase output voltages of the wye-connected autotransformer can be expressed as

$$\begin{cases} u_{a1} = \sqrt{2}U_n \sin(\omega t + 15^\circ) \\ u_{b1} = \sqrt{2}U_n \sin(\omega t - 120^\circ + 15^\circ) \\ u_{c1} = \sqrt{2}U_n \sin(\omega t + 120^\circ + 15^\circ), \end{cases} \tag{3}$$

$$\begin{cases} u_{a2} = \sqrt{2}U_n \sin(\omega t - 15^\circ) \\ u_{b2} = \sqrt{2}U_n \sin(\omega t - 120^\circ - 15^\circ) \\ u_{c2} = \sqrt{2}U_n \sin(\omega t + 120^\circ - 15^\circ), \end{cases} \tag{4}$$

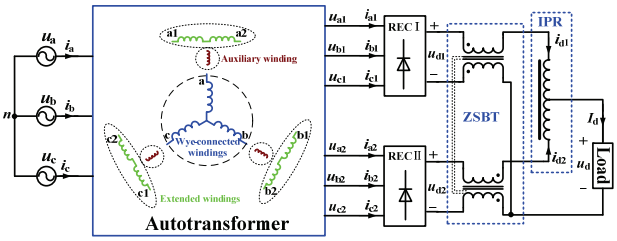

Fig. 1. 12-pulse rectifier with wye-connected autotransformer.

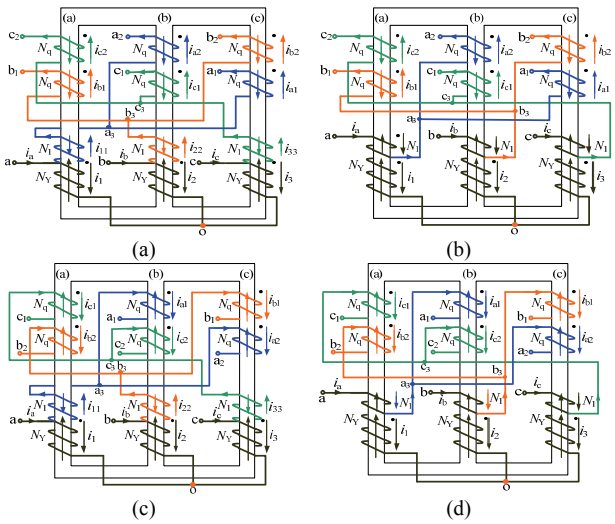

Fig. 2. Winding configurations of the wye-connected autotransformer under different k_1 and k_2 values. (a) $k_1 \geq 0$ and $k_2 \geq 0$. (b) $k_1 \leq 0$ and $k_2 \geq 0$. (c) $k_1 \geq 0$ and $k_2 \leq 0$. (d) $k_1 \leq 0$ and $k_2 \leq 0$.

where U_n represents the amplitude of the three-phase output voltage.

III. Winding Configurations of the Wye-Connected Autotransformer

The windings of the wye-connected autotransformer can be divided into three types, namely, wye-connected, auxiliary, and extended windings, as shown in Fig. 1. On the basis of positional relations, four winding configurations of the wye-connected autotransformer are available, as shown in Fig. 2. Fig. 3 presents the corresponding phasor diagrams of these winding configurations.

In Fig. 3, with phase **a** as an example, $\dot{U}_a$ is the phasor of the input phase voltage u_a; $\dot{U}_{a1}$ and $\dot{U}_{a2}$ denote the phasors of output voltages u_{a1} and u_{a2}, respectively. Given the wye connection of the winding configuration, the voltage across the wye-connected winding is equal to u_a, the voltage across the auxiliary winding is equal to u_{a3a}, and the voltage across the extended winding is equal to u_{a1a3}.

In Figs. 3(a) and 3(b), $\dot{U}_c$, $\dot{U}_{a1a3}$, $\dot{U}_{a1a}$, and $\dot{U}_{a3a}$ are the phasors of output voltages u_c, u_{a1a3}, u_{a1a}, and u_{a3a}, respectively. Figs. 3(a) and 3(b) show that $\dot{U}_{a1a3}$ is parallel to $\dot{U}_c$, and

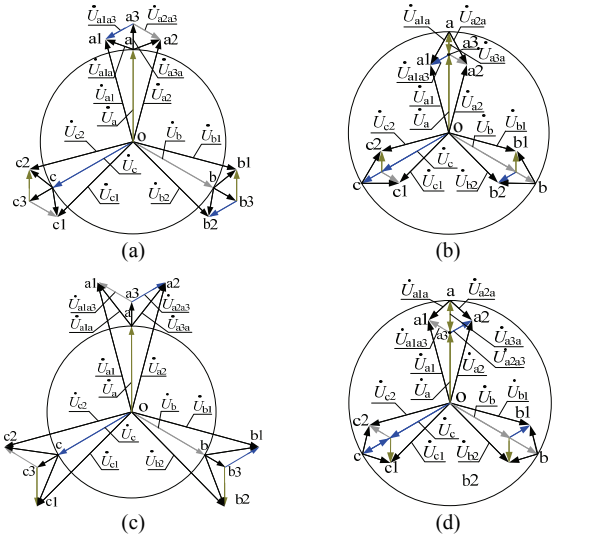

Fig. 3. Phasor diagram of the wye-connected autotransformer under different k_1 and k_2 values. (a) $k_1 \geq 0$ and $k_2 \geq 0$. (b) $k_1 \leq 0$ and $k_2 \geq 0$. (c) $k_1 \geq 0$ and $k_2 \leq 0$. (d) $k_1 \leq 0$ and $k_2 \leq 0$.

$\dot{U}_{a3a}$ is parallel to $\dot{U}_a$, respectively. The relation among $\dot{U}_a$, $\dot{U}_{a1}$, $\dot{U}_{a3a}$, $\dot{U}_{a1a3}$, and $\dot{U}_{a1a}$ meets

$$\begin{cases} \dot{U}_{a1} = \dot{U}_a + \dot{U}_{a1a} \\ \dot{U}_{a1a} = \dot{U}_{a3a} + \dot{U}_{a1a3} \\ \dot{U}_{a1a} = k_1 \dot{U}_a + k_2 \dot{U}_c \end{cases}. \tag{5}$$

Figs. 3(c) and 3(d) illustrate that $\dot{U}_{a1a3}$ is parallel to $\dot{U}_b$, and $\dot{U}_{a3a}$ is parallel to $\dot{U}_a$, respectively. The relation among $\dot{U}_a$, $\dot{U}_{a1}$, $\dot{U}_{a3a}$, $\dot{U}_{a1a3}$, and $\dot{U}_{a1a}$ meets

$$\begin{cases} \dot{U}_{a1} = \dot{U}_a + \dot{U}_{a1a} \\ \dot{U}_{a1a} = \dot{U}_{a3a} + \dot{U}_{a1a3} \\ \dot{U}_{a1a} = k_1 \dot{U}_a + k_2 \dot{U}_b \end{cases}, \tag{6}$$

where k_1 represents the position parameter of the auxiliary winding, which reflects the position relative to the wye-connected windings and turn numbers of the auxiliary winding, and k_2 refers to the proportional parameter of the extended winding, which reflects the polarity relative to the wye-connected windings and turn numbers of the extended winding.

In Eq. (6), k_1 and k_2 are scalars, which can be greater or smaller than zero. As shown in Fig. 2 and Fig. 3, to set phase **a** as an example, when k_1 is greater than zero, $\dot{U}_{a3a}$ is in the direction of $\dot{U}_a$; the auxiliary winding **a3a** and wye-connected winding **ao** are different and connected to point **a**. When k_1 is less than zero, $\dot{U}_{a3a}$ is opposite to $\dot{U}_a$; the auxiliary winding **a3a** is part of wye-connected winding **ao**. When k_2 is greater than zero, $\dot{U}_{a1a3}$ and $\dot{U}_{a2a3}$ are parallel to $\dot{U}_c$ and $\dot{U}_b$, respectively; the extended winding and corresponding wye-connected winding have the same polarity. When k_2 is lower than zero, $\dot{U}_{a1a3}$ and $\dot{U}_{a2a3}$ are opposite to $\dot{U}_b$ and $\dot{U}_c$, respectively; the extended winding and corresponding wye-connected winding have opposite polarity.

As shown in Figs. 2(a) and 3(a), when $k_1 \geq 0$ and $k_2 \geq 0$, the relation among N_1, N_Y, N_q, k_1, and k_2 meets

$$\frac{N_1}{N_Y} = k_1 \qquad \frac{N_q}{N_Y} = k_2 , \tag{7}$$

where N_Y is the turn number of the wye-connected winding, N_1 represents the turn number of the auxiliary winding, and N_q denotes the turn number of the extended winding.

As shown in Figs. 2(b) and 3(b), when $k_1 \leq 0$ and $k_2 \geq 0$, the relation among N_1, N_Y, N_q, k_1, and k_2 meets

$$\frac{N_1}{N_Y} = -k_1 \qquad \frac{N_q}{N_Y} = k_2 . \tag{8}$$

As shown in Figs. 2(c) and 3(c), when $k_1 \geq 0$ and $k_2 \leq 0$, the relation among N_1, N_Y, N_q, k_1, and k_2 meets

$$\frac{N_1}{N_Y} = k_1 \qquad \frac{N_q}{N_Y} = -k_2 . \tag{9}$$

As shown in Figs. 2(d) and 3(d), when $k_1 \leq 0$ and $k_2 \leq 0$, the relation among N_1, N_Y, N_q, k_1, and k_2 meets

$$\frac{N_1}{N_Y} = -k_1 \qquad \frac{N_q}{N_Y} = -k_2 . \tag{10}$$

On the basis of Eqs. (5) and (6), the wye-connected, auxiliary, and extended windings are duly connected to produce output voltages with an appropriate phase-shift angle. Therefore, to achieve the phase-shift angle, k_1 and k_2 should meet some expressions.

A. Constraint Condition Between Parameters

Assume that U_m is equal to 1. The turn ratio of the wye-connected autotransformer is defined as

$$k = \frac{U_{a1}}{U_a} = \frac{U_n}{U_m} = U_n . \tag{11}$$

Fig. 3(a) shows the phasor diagram when $k_1 \geq 0$ and $k_2 \geq 0$. Triangle **oa1a3** proves that

$$\frac{k_2}{\sin 15^\circ} = \frac{1+k_1}{\sin 105^\circ} = \frac{U_{a1}}{\sin 60^\circ} = \frac{k}{\sin 60^\circ} . \tag{12}$$

Fig. 3(b) presents the phasor diagram when $k_1 \leq 0$ and $k_2 \geq 0$. Triangle **oa1a3** shows that

$$\frac{k_2}{\sin 15^\circ} = \frac{1+k_1}{\sin 105^\circ} = \frac{U_{a1}}{\sin 60^\circ} = \frac{k}{\sin 60^\circ} . \tag{13}$$

On the basis of Eqs. (12) and (13), when $k_2 \geq 0$, k_2 and k can be expressed as

$$\begin{cases} k_2 = (2-\sqrt{3})(1+k_1) \\ k = \dfrac{\sqrt{6}}{2}(\sqrt{3}-1)(1+k_1) \end{cases}. \tag{14}$$

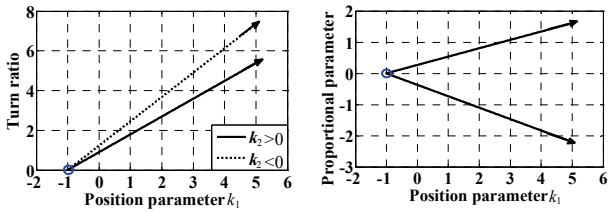

(a) (b)

Fig. 4. Relation among k_1, k_2, and k. (a) Relation diagram between k_1 and k_2. (b) Relation between k_1 and k.

Fig. 3(c) displays the phasor diagram when $k_1 \geq 0$ and $k_2 \leq 0$. Triangle **oa1a3** demonstrates that

$$\frac{-k_2}{\sin 15^\circ} = \frac{1+k_1}{\sin 45^\circ} = \frac{U_{a1}}{\sin 120^\circ} = \frac{k}{\sin 120^\circ}. \quad (15)$$

Fig. 3(d) exhibits the phasor diagram when $k_1 \leq 0$ and $k_2 \leq 0$. Triangle **oa1a3** establishes that

$$\frac{-k_2}{\sin 15^\circ} = \frac{1+k_1}{\sin 45^\circ} = \frac{U_{a1}}{\sin 120^\circ} = \frac{k}{\sin 120^\circ}. \quad (16)$$

On the basis of Eqs. (15) and (16), when $k_2 \leq 0$, k_2 and k can be expressed as

$$\begin{cases} k_2 = -\dfrac{(\sqrt{3}-1)}{2}(1+k_1) \\ k = \dfrac{\sqrt{6}}{2}(1+k_1) \end{cases}. \quad (17)$$

As shown in Fig. 3, k_1 should be greater than −1. Fig. 4(a) presents the relation between k_1 and k_2, whereas Fig. 4(b) visualizes the relation between k_1 and turn ratio k.

B. Currents Through Windings under Different Winding Configurations

The current through the windings under different winding configurations is calculated.

In Fig. 2(a), from the Ampere-turn equal law,

$$\begin{cases} N_q i_{c2} + N_q i_{b1} + N_1 i_{11} = N_Y i_1 \\ N_q i_{a2} + N_q i_{c1} + N_1 i_{22} = N_Y i_2 \\ N_q i_{b2} + N_q i_{a1} + N_1 i_{33} = N_Y i_3 \end{cases}. \quad (18)$$

From Kirchhoff's current law,

$$\begin{cases} i_a = i_{11} + i_1 \\ i_b = i_{22} + i_2 \\ i_c = i_{33} + i_3 \end{cases} \quad \begin{cases} i_{11} = i_{a2} + i_{a1} \\ i_{22} = i_{b2} + i_{b1} \\ i_{33} = i_{c2} + i_{c1} \end{cases}. \quad (19)$$

Therefore, to set the core limb **(a)** as an example, the currents through the auxiliary and extended windings and the input line current i_a are calculated as

$$\begin{cases} i_1 = \dfrac{N_q}{N_Y} i_{c2} + \dfrac{N_q}{N_Y} i_{b1} + \dfrac{N_1}{N_Y}(i_{a2} + i_{a1}) \\ i_{11} = i_{a2} + i_{a1} \\ i_a = i_{a2} + i_{a1} + \dfrac{N_q}{N_Y} i_{c2} + \dfrac{N_q}{N_Y} i_{b1} + \dfrac{N_1}{N_Y}(i_{a2} + i_{a1}) \end{cases}. \quad (20)$$

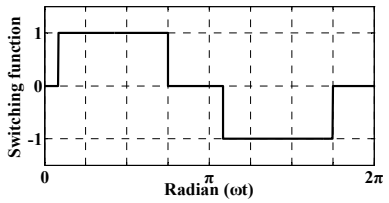

Fig. 5. Switching function of S_{a1}.

Substituting Eq. (7) into Eq. (20) yields

$$\begin{cases} i_1 = k_2(i_{c2} + i_{b1}) + k_1(i_{a2} + i_{a1}) \\ i_{11} = i_{a2} + i_{a1} \\ i_a = (1+k_1)(i_{a2} + i_{a1}) + k_2(i_{c2} + i_{b1}) \end{cases}. \quad (21)$$

Under large inductive load, the load current can be assumed to be a constant value I_d, and the output currents of the bridge rectifiers can be expressed as

$$i_{d1} = i_{d2} = 0.5 I_d. \quad (22)$$

Output currents i_{a1}, i_{b1}, i_{c1}, i_{a2}, i_{b2}, and i_{c2} of the autotransformer meet

$$\begin{cases} i_{a1} = S_{a1} i_{d1} \\ i_{b1} = S_{b1} i_{d1} \\ i_{c1} = S_{c1} i_{d1} \end{cases} \quad \begin{cases} i_{a2} = S_{a2} i_{d1} \\ i_{b2} = S_{b2} i_{d1} \\ i_{c2} = S_{c2} i_{d1} \end{cases}, \quad (23)$$

where S_{a1}, S_{b1}, S_{c1}, S_{a2}, S_{b2}, and S_{c2} are the switching functions of phases **a1**, **b1**, **c1**, **a2**, **b2**, and **c2**, respectively.

Fig. 5 illustrates switching function S_{a1} when the three-phase output voltages of the autotransformer meet Eqs. (3) and (4). The relation among the switching functions meets

$$\begin{cases} S_{b1} = S_{a1} \angle -120^\circ \\ S_{c1} = S_{a1} \angle +120^\circ \end{cases} \quad \begin{cases} S_{a2} = S_{a1} \angle -30^\circ \\ S_{b2} = S_{b1} \angle -30^\circ \\ S_{c2} = S_{c1} \angle -30^\circ \end{cases}. \quad (24)$$

Substituting Eqs. (7) and (23) into Eq. (21) yields

$$\begin{cases} i_1 = 0.5 I_d [k_2(S_{c2} + S_{b1}) + k_1(S_{a2} + S_{a1})] \\ i_{11} = 0.5 I_d (S_{a1} + S_{a2}) \\ i_a = 0.5 I_d [(1+k_1)(S_{a2} + S_{a1}) + k_2(S_{c2} + S_{b1})] \end{cases}. \quad (25)$$

Fig. 6 shows currents i_1 and i_{11}, the input line current, and the spectrum when $k_1 = 1$ and $k_2 = 2(2-\sqrt{3})$.

Similarly, as shown in Figs. 2(b) and 3(b), when $k_1 \leq 0$ and $k_2 \geq 0$, the currents through the wye-connected and auxiliary windings can be calculated as

$$\begin{cases} i_1 = 0.5 I_d [k_2(S_{c2} + S_{b1}) + k_1(S_{a2} + S_{a1})] \\ i_a = 0.5 I_d [k_2(S_{c2} + S_{b1}) + (1+k_1)(S_{a2} + S_{a1})] \end{cases}. \quad (26)$$

Fig. 7 shows currents i_1 and i_a and the spectrum of the input line current when $k_1 = -0.5$ and $k_2 = 0.5 \times (2-\sqrt{3})$.

Similarly, as shown in Figs. 2(c) and 3(c), when $k_1 \geq 0$ and $k_2 \leq 0$, the currents through the auxiliary and extended windings and input line current i_a are calculated as

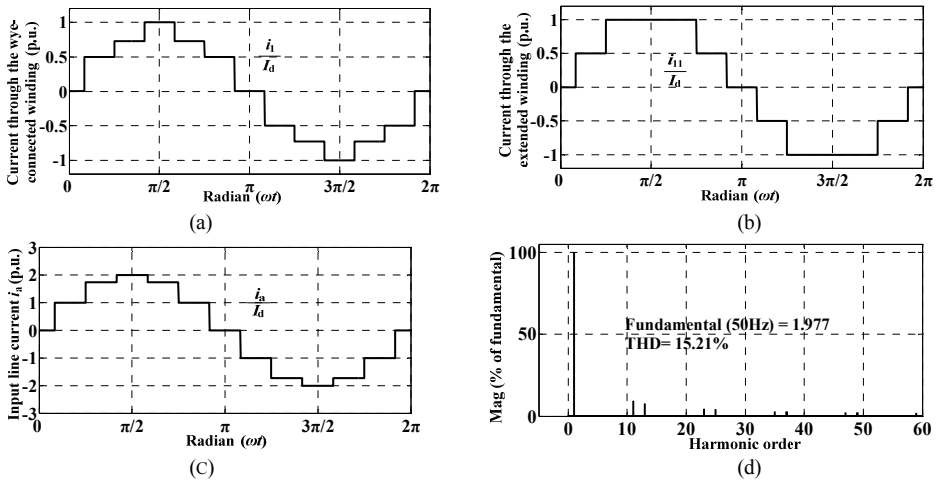

Fig. 6. Currents through the windings and input line current when $k_1 = 1$ and $k_2 = 2(2-\sqrt{3})$. (a) Current through the wye-connected winding. (b) Current through the extended winding. (c) Input line current and (d) its spectrum.

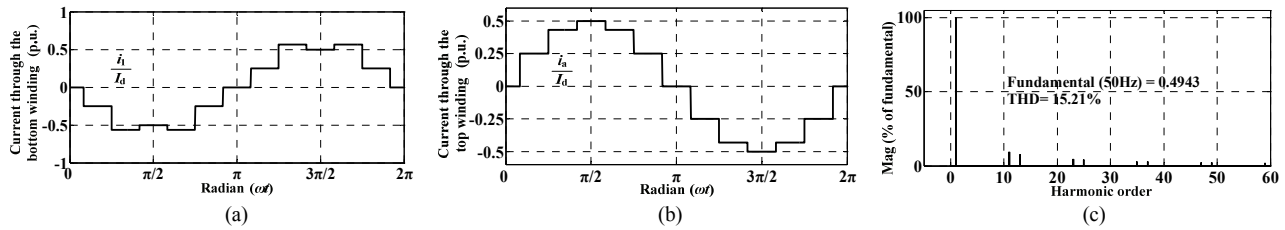

Fig. 7. Currents through the windings and input line current when $k_1 = -0.5$ and $k_2 = 0.5\times(2-\sqrt{3})$. (a) Current through the bottom winding of the wye-connected winding. (b) Current through the top winding of the wye-connected winding, which is also the input line current. (c) Spectrum of the input line current.

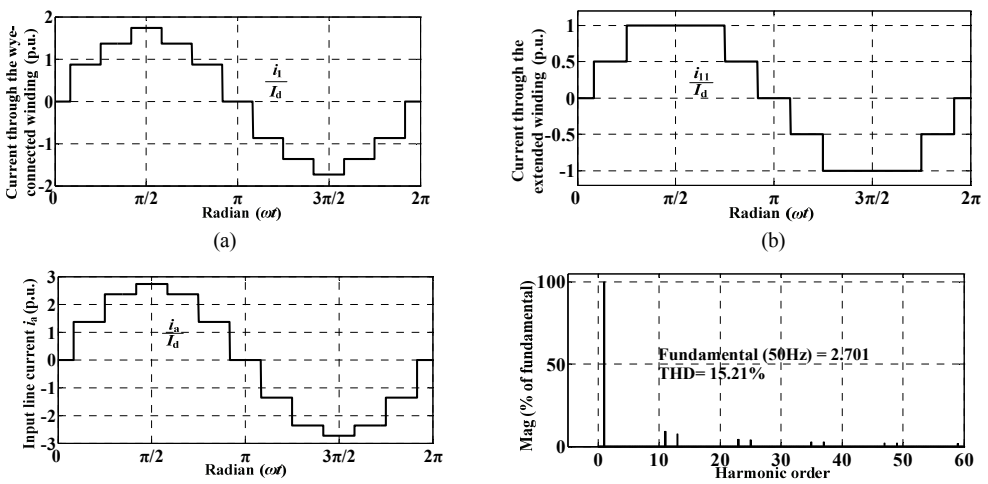

Fig. 8. Currents through the windings and input line current when $k_1 = 1$ and $k_2 = (1-\sqrt{3})$. (a) Current through the wye-connected winding. (b) Current through the extended winding. (c) Input line current and (d) its spectrum.

$$\begin{cases} i_1 = 0.5I_d[k_1(S_{a2}+S_{a1}) + k_2(S_{c1}+S_{b2})] \\ i_{11} = 0.5I_d(S_{a2}+S_{a1}) \\ i_a = 0.5I_d[(1+k_1)(S_{a2}+S_{a1}) + k_2(S_{c1}+S_{b2})]. \end{cases} \quad (27)$$

Fig. 8 shows currents i_1 and i_{11}, input line current, and the spectrum when $k_1 = 1$ and $k_2 = (1-\sqrt{3})$.

Similarly, as shown in Figs. 2(d) and 3(d), when $k_1 \le 0$ and $k_2 \le 0$, the currents through the wye-connected and auxiliary windings are calculated as

$$\begin{cases} i_1 = 0.5I_d[k_1(S_{a2}+S_{a1}) + k_2(S_{c1}+S_{b2})] \\ i_a = 0.5I_d[(1+k_1)(S_{a2}+S_{a1}) + k_2(S_{c1}+S_{b2})]. \end{cases} \quad (28)$$

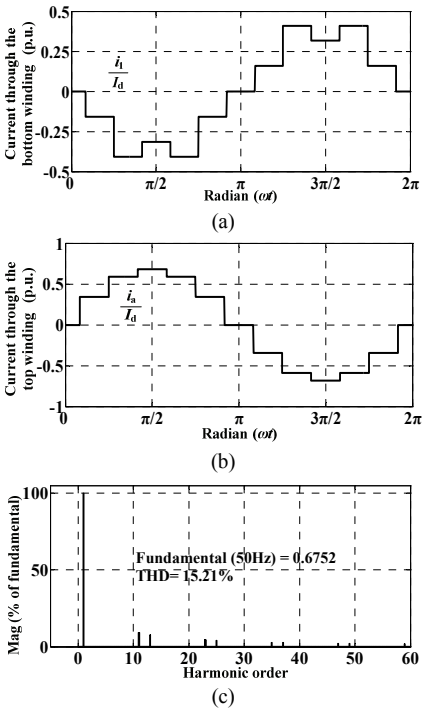

Fig. 9. Currents through the windings and input line current when $k_1 = -0.5$ and $k_2 = (1-\sqrt{3})/4$. (a) Current through the bottom winding of the wye-connected winding. (b) Current through the top winding of the wye-connected winding, which is also the input line current. (c) Spectrum of the input line current.

Fig. 9 shows currents i_1 and i_a and the spectrum of i_a when $k_1 = -0.5$ and $k_2 = 0.25 \times (1-\sqrt{3})$.

Figs. 6(d), 7(c), 8(d), and 9(c) show that the THD of the input line current is approximately 15.21% under different winding configurations, and the winding configuration does not affect the THD.

IV. Relation between Configuration Parameter and kVA Rating

The kilovolt-ampere rating of the autotransformer is determined by the voltage across and current through the windings. The kilovolt-ampere rating can be expressed as

$$S_{\mathrm{kVA}} = 0.5\sum UI \,, \tag{29}$$

where U and I are the voltage across and current through the windings of the transformer.

In accordance with modulation theory, the output voltages of the two bridge rectifiers can be expressed as

$$\begin{cases} u_{\mathrm{d1}} = u_{\mathrm{a1}}S_{\mathrm{a1}} + u_{\mathrm{b1}}S_{\mathrm{b1}} + u_{\mathrm{c1}}S_{\mathrm{c1}} \\ u_{\mathrm{d2}} = u_{\mathrm{a2}}S_{\mathrm{a2}} + u_{\mathrm{b2}}S_{\mathrm{b2}} + u_{\mathrm{c2}}S_{\mathrm{c2}} \end{cases}. \tag{30}$$

On the basis of Fig. 1, the load voltage can be expressed as

$$u_{\mathrm{d}} = 0.5(u_{\mathrm{d1}} + u_{\mathrm{d2}}) \,. \tag{31}$$

From Eqs. (2)-(4), (11), and (14), when $k_2 \geq 0$, the relation between U_{n} and U_{m} meets

$$U_{\mathrm{n}} = \frac{\sqrt{6}}{2}(\sqrt{3}-1)(1+k_1)U_{\mathrm{m}} \,. \tag{32}$$

Therefore, when $k_2 \geq 0$, the two groups of three-phase output voltages can be expressed as

$$\begin{cases} \begin{cases} u_{\mathrm{a1}} = (3-\sqrt{3})(1+k_1)U_{\mathrm{m}}\sin(\omega t + 15^{\mathrm{o}}) \\ u_{\mathrm{b1}} = (3-\sqrt{3})(1+k_1)U_{\mathrm{m}}\sin(\omega t - 105^{\mathrm{o}}) \\ u_{\mathrm{c1}} = (3-\sqrt{3})(1+k_1)U_{\mathrm{m}}\sin(\omega t + 135^{\mathrm{o}}) \end{cases} \\ \begin{cases} u_{\mathrm{a2}} = (3-\sqrt{3})(1+k_1)U_{\mathrm{m}}\sin(\omega t - 15^{\mathrm{o}}) \\ u_{\mathrm{b2}} = (3-\sqrt{3})(1+k_1)U_{\mathrm{m}}\sin(\omega t - 135^{\mathrm{o}}) \\ u_{\mathrm{c2}} = (3-\sqrt{3})(1+k_1)U_{\mathrm{m}}\sin(\omega t + 105^{\mathrm{o}}) \end{cases} \end{cases}. \tag{33}$$

From Eqs. (24) and (30)–(33), when $k_2 \geq 0$, load voltage u_{d} is calculated as

$$u_{\mathrm{d}} = \begin{cases} \dfrac{3}{\sqrt{2}}(1+k_1)U_{\mathrm{m}}\cos(\omega t - k30^{\mathrm{o}}) \\ \quad \omega t \in [k15^{\mathrm{o}} \quad (k+1)15^{\mathrm{o}}], k = 0,1,2,3... \\ \dfrac{3}{\sqrt{2}}(1+k_1)U_{\mathrm{m}}\cos(\omega t - k30^{\mathrm{o}} - 30^{\mathrm{o}}) \\ \quad \omega t \in [(k+1)15^{\mathrm{o}} \quad (k+2)15^{\mathrm{o}}], k = 0,1,2,3... \end{cases}. \tag{34}$$

From Eq. (34), when $k_2 \geq 0$, the RMS value of load voltage is as follows:

$$U_{\mathrm{d}} = 1.5\sqrt{(\pi+3)/\pi}(1+k_1)U_{\mathrm{m}} \,. \tag{35}$$

From Eqs. (2)-(4), (11), and (17), when $k_2 \leq 0$, the relation between U_{n} and U_{m} meets

$$U_{\mathrm{n}} = \frac{\sqrt{6}}{2}(1+k_1)U_{\mathrm{m}} \,. \tag{36}$$

Therefore, when $k_2 \leq 0$, the two groups of three-phase output voltages can be expressed as

$$\begin{cases} \begin{cases} u_{\mathrm{a1}} = \sqrt{3}(1+k_1)U_{\mathrm{m}}\sin(\omega t + 15^{\mathrm{o}}) \\ u_{\mathrm{b1}} = \sqrt{3}(1+k_1)U_{\mathrm{m}}\sin(\omega t - 105^{\mathrm{o}}) \\ u_{\mathrm{c1}} = \sqrt{3}(1+k_1)U_{\mathrm{m}}\sin(\omega t + 135^{\mathrm{o}}) \end{cases} \\ \begin{cases} u_{\mathrm{a2}} = \sqrt{3}(1+k_1)U_{\mathrm{m}}\sin(\omega t - 15^{\mathrm{o}}) \\ u_{\mathrm{b2}} = \sqrt{3}(1+k_1)U_{\mathrm{m}}\sin(\omega t - 135^{\mathrm{o}}) \\ u_{\mathrm{c2}} = \sqrt{3}(1+k_1)U_{\mathrm{m}}\sin(\omega t + 105^{\mathrm{o}}) \end{cases} \end{cases}. \tag{37}$$

From Eqs. (24), (30), (31), and (37), when $k_2 \leq 0$, the load voltage u_{d} is calculated as

$$u_{\mathrm{d}} = \begin{cases} \dfrac{3\sqrt{2}}{4}(\sqrt{3}+1)(1+k_1)U_{\mathrm{m}}\cos(\omega t - k30^{\mathrm{o}}) \\ \quad \omega t \in [k15^{\mathrm{o}} \quad (k+1)15^{\mathrm{o}}], k = 0,1,2,3... \\ \dfrac{3\sqrt{2}}{4}(\sqrt{3}+1)(1+k_1)U_{\mathrm{m}}\cos(\omega t - k30^{\mathrm{o}} - 30^{\mathrm{o}}) \\ \quad \omega t \in [(k+1)15^{\mathrm{o}} \quad (k+2)15^{\mathrm{o}}], k = 0,1,2,3... \end{cases}. \tag{38}$$

From Eq. (38), when $k_2 \leq 0$, the RMS value of the load

voltage is as follows:

$$U_{\mathrm{d}}=\frac{3\sqrt{\pi+3}}{2(\sqrt{3}-1)\sqrt{\pi}}(1+k_1)U_{\mathrm{m}}. \tag{39}$$

The currents through the extended windings are equal to i_{a1}, i_{b1}, i_{c1}, i_{a2}, i_{b2}, and i_{c2}. Therefore, the RMS values of the currents through the extended windings are calculated as

$$I_{\mathrm{a1}}=I_{\mathrm{b1}}=I_{\mathrm{c1}}=I_{\mathrm{a2}}=I_{\mathrm{b2}}=I_{\mathrm{c2}}=\frac{\sqrt{6}}{6}I_{\mathrm{d}}. \tag{40}$$

The detailed calculation processes of the kVA rating of the wye-connected autotransformer when $k_1\geq 0$ and $k_2\geq 0$ are shown as follows.

When $k_1\geq 0$ and $k_2\geq 0$, the voltages across the wye-connected windings are the three-phase input voltages, and their RMS value is equal to U_{m}. From Eq. (22), the RMS values of the currents through the wye-connected windings are as follows:

$$I_1=I_{\mathrm{d}}\sqrt{\frac{7k_1^2-4k_1k_2+k_2^2}{12}}. \tag{41}$$

On the basis of the definition of position parameter, the RMS value of the voltage across the auxiliary winding is equal to k_1U_{m}. Moreover, from Eq. (25), the RMS value of the current through the auxiliary winding is as follows:

$$I_{11}=\sqrt{\frac{7}{12}}I_{\mathrm{d}}. \tag{42}$$

On the basis of the definition of proportional parameter, the RMS value of the voltage across the extended winding is equal to k_2U_{m}, and the current through the extended winding meets Eq. (40).

Therefore, when $k_1\geq 0$ and $k_2\geq 0$, the kVA rating is calculated as

$$S_{\mathrm{kVA1}}=\frac{\sqrt{3}}{4}(\sqrt{7k_1^2-4k_1k_2+k_2^2}+\sqrt{7}k_1+2\sqrt{2}k_2)U_{\mathrm{m}}I_{\mathrm{d}}. \tag{43}$$

On the basis of Eq. (35), S_{kVA1} can also be expressed as

$$S_{\mathrm{kVA1}}=\frac{\sqrt{3\pi}U_{\mathrm{d}}I_{\mathrm{d}}(\sqrt{7k_1^2-4k_1k_2+k_2^2}+\sqrt{7}k_1+2\sqrt{2}k_2)}{6\sqrt{\pi+3}(1+k_1)}. \tag{44}$$

The load power is defined as

$$P_{\mathrm{o}}=U_{\mathrm{d}}I_{\mathrm{d}}. \tag{45}$$

Substituting Eq. (30) into Eq. (44) yields

$$S_{\mathrm{kVA1}}=\frac{\sqrt{3\pi}(\sqrt{7k_1^2-4k_1k_2+k_2^2}+\sqrt{7}k_1+2\sqrt{2}k_2)}{6\sqrt{\pi+3}(1+k_1)}P_{\mathrm{o}}. \tag{46}$$

The equivalent kVA rating $S_{\mathrm{eq,kVA}}$ is expressed as

$$S_{\mathrm{eq,kVA}}=\frac{S_{\mathrm{kVA}}}{P_{\mathrm{o}}}. \tag{47}$$

$S_{\mathrm{eq,kVA}}$ describes the relation between the kVA rating and configuration parameter under the same load power.

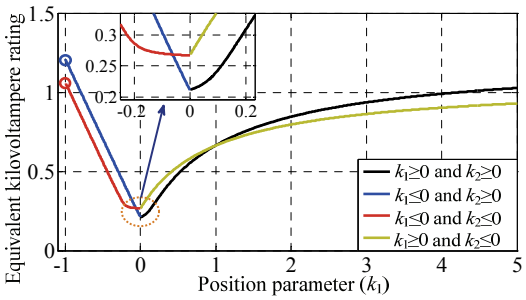

Fig. 10. Equivalent kVA rating under different k_1 and k_2 values.

From Eqs. (46) and (47), when $k_1\geq 0$ and $k_2\geq 0$, the equivalent kVA rating is as follows

$$S_{\mathrm{eq,kVA1}}=\frac{\sqrt{3\pi}(\sqrt{7k_1^2-4k_1k_2+k_2^2}+\sqrt{7}k_1+2\sqrt{2}k_2)}{6\sqrt{\pi+3}(1+k_1)}. \tag{48}$$

Similarly, when $k_1\leq 0$ and $k_2\geq 0$, the equivalent kVA rating is calculated as

$$\begin{aligned}S_{\mathrm{eq,kVA2}}=&\frac{\sqrt{3\pi}}{6\sqrt{\pi+3}(1+k_1)}[(1+k_1)\sqrt{7k_1^2-4k_1k_2+k_2^2}\\&-k_1\sqrt{7k_1^2-4k_1k_2+k_2^2+14k_1-4k_2+7}+2\sqrt{2}k_2].\end{aligned} \tag{49}$$

When $k_1\geq 0$ and $k_2\leq 0$, the equivalent kVA rating is calculated as

$$S_{\mathrm{eq,kVA3}}=\frac{\sqrt{\pi}(\sqrt{7k_1^2-10k_1k_2+4k_2^2}+\sqrt{7}k_1-2\sqrt{2}k_2)}{(3+\sqrt{3})\sqrt{\pi+3}(1+k_1)}. \tag{50}$$

When $k_1\leq 0$ and $k_2\leq 0$, the equivalent kVA rating is calculated as

$$\begin{aligned}S_{\mathrm{eq,kVA4}}=&\frac{\sqrt{3\pi}(\sqrt{3}-1)}{6\sqrt{\pi+3}(1+k_1)}[(1+k_1)\sqrt{7k_1^2-10k_1k_2+4k_2^2}\\&-k_1\sqrt{7k_1^2-10k_1k_2+4k_2^2+14k_1-10k_2+7}-2\sqrt{2}k_2].\end{aligned} \tag{51}$$

From Eqs. (48), (49), (50), and (51), the equivalent kVA rating under different k_1 and k_2 values is obtained, as shown in Fig. 10.

From Fig. 10, conclusions can be obtained as follows.

(1) When $k_2\geq 0$ and $k_1=0$, $S_{\mathrm{eq,kVA}}$ is minimal, and the minimum is 0.2118. Therefore, when $k_2\geq 0$ and $k_1=0$, the kilovolt-ampere rating of the wye-connected autotransformer is approximately 21% of the load power. Fig. 11 shows the winding configuration and phasor diagram of the autotransformer when $k_2\geq 0$ and $k_1=0$. In comparison with other winding configurations when $k_2\geq 0$ as shown in Figs. 2(a) and 2(b), the autotransformer has the simplest winding configuration when $k_2\geq 0$ and $k_1=0$. In addition, every core limb only has three windings. When $k_2\geq 0$ and $k_1=0$, the wye-connected autotransformer has the optimal configuration.

(2) When $k_2\geq 0$ and $k_1=0$, $k=\sqrt{6}(\sqrt{3}-1)/2$, which is less than one. Therefore, the autotransformer operates

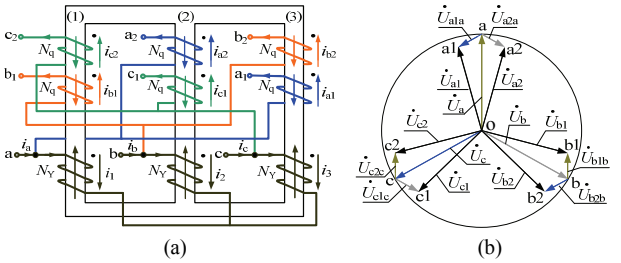

(a) (b)

Fig. 11 Winding configuration and phasor diagram of the autotransformer when $k_2 \geq 0$ and $k_1 = 0$. (a) Winding configuration. (b) Phasor diagram.

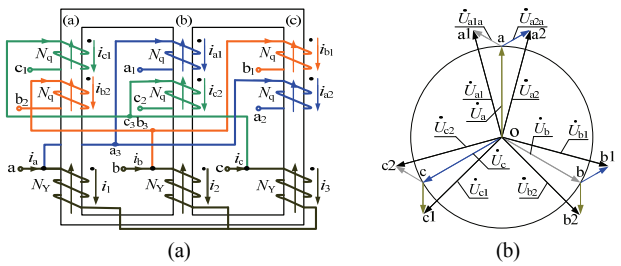

(a) (b)

Fig. 12. Winding configuration and phasor diagram of the autotransformer when $k_2 \leq 0$ and $k_1 = 0$. (a) Winding configuration. (b) Phasor diagram.

under a step-down condition in this case. When $k_2 \geq 0$ and $k_1 = 0$, $k_2 = (2-\sqrt{3})$. Therefore, the ratio of N_Y to N_q in Fig. 11 (a) is $1/(2-\sqrt{3})$.

(3) When the configuration of the wye-connected autotransformer is optimal, the turn ratio k is constant, indicating that the output voltages of the wye-connected autotransformer are constant. When various output voltages are required, the desired turn ratio is different from the optimal turn ratio. Furthermore, the appropriate k_1 and k_2 should be selected from Eqs. (14) and (17), respectively. In this manner, the configuration of the wye-connected autotransformer is not optimal.

(4) In fact, when $k_2 \leq 0$ and $k_1 = 0$, the autotransformer has the simplest winding configuration, and every core limb only has three windings. Fig. 12 shows the winding configuration and phasor diagram when $k_2 \leq 0$ and $k_1 = 0$, wherein the equivalent kilovolt-ampere rating of the autotransformer is approximately 0.2671. This value is greater than that of the autotransformer when $k_2 \geq 0$ and $k_1 = 0$. Therefore, in the viewpoint of simplest winding configuration and least equivalent kilovolt-ampere rating, the winding configuration shown in Fig. 11(a) is optimal.

V. Experimental Validation

In this section, eight wye-connected autotransformers with different connections under various input voltages and loads are designed to verify the previous theoretical analysis. Fig. 13 shows pictures of the prototype.

(a) (b) (c) (d) (e) (f) (g) (h)

Fig. 13. Pictures of the wye-connected autotransformers. (a) $k_2 \geq 0$ and $k_1 = -0.5$. (b) $k_2 \geq 0$ and $k_1 = 0$. (c) $k_2 \geq 0$ and $k_1 = 0.5$. (d) $k_2 \geq 0$ and $k_1 = 1$. (e) $k_2 \leq 0$ and $k_1 = -0.5$. (f) $k_2 \leq 0$ and $k_1 = 0$. (g) $k_2 \leq 0$ and $k_1 = 0.5$. (h) $k_2 \leq 0$ and $k_1 = 1$.

Experimental results are shown as follows:

(1) $k_2 \geq 0$ and $k_1 = -0.5$: Fig. 14 shows the voltages across and current through the windings of core limb (a) and the load current and voltage when $k_2 \geq 0$ and $k_1 = -0.5$. Assume that the autotransformer is symmetrical. The apparent power of the autotransformer is equal to 738.6 VA, and the load power is 1014.3 W. Therefore, the equivalent kVA is 0.728.

(2) $k_2 \geq 0$ and $k_1 = 0$: Fig. 15 shows the voltages across and current through the windings of core limb (a) and the load current and voltage when $k_2 \geq 0$ and $k_1 = 0$. The

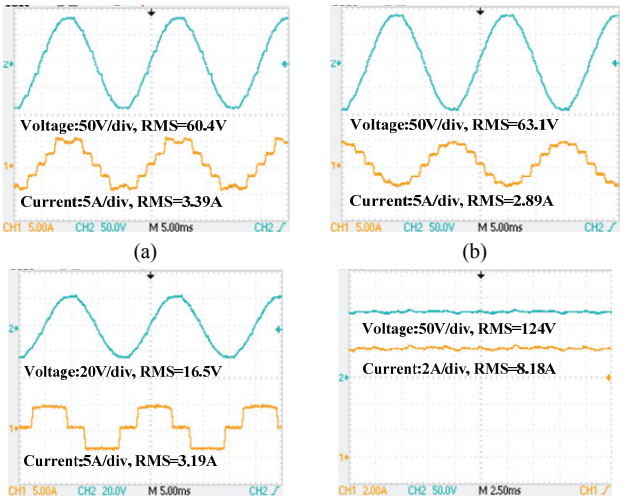

Fig. 14. Voltage and current. (a) Through the wye-connected winding **ao**. (b) Through auxiliary winding **aa3**. (c) Extended winding **b1b3**. (d) The load voltage and current when $k_2 \geq 0$ and $k_1 = -0.5$.

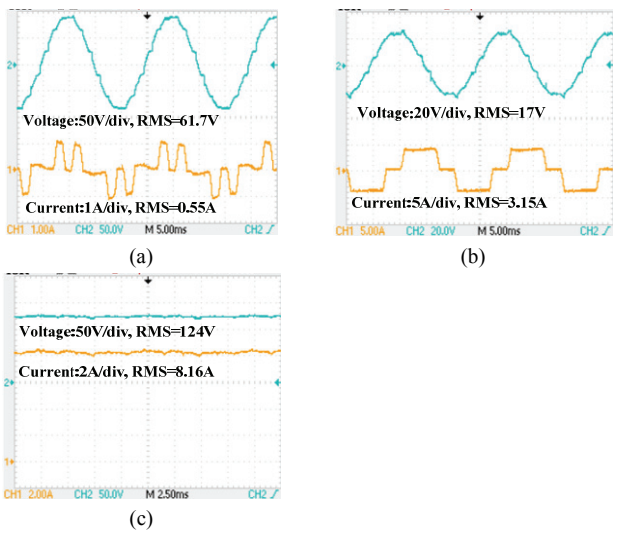

Fig. 15. Voltage and current. (a) Through the wye-connected winding **ao**. (b) Extended winding **b1b**. (c) The load voltage and current when $k_2 \geq 0$ and $k_1 = 0$.

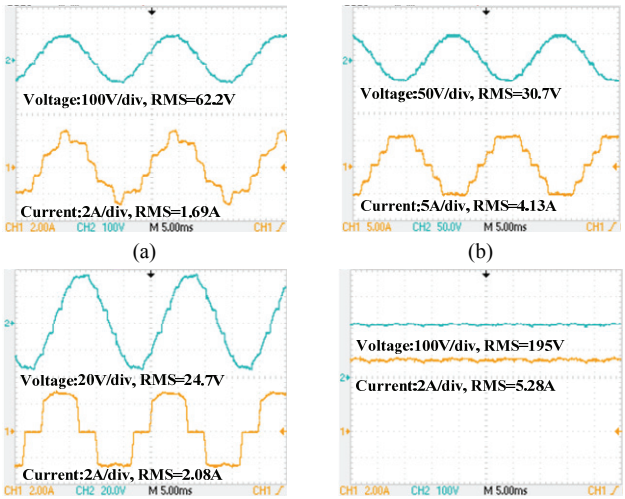

Fig. 16. Voltage and current. (a) Through the wye-connected winding **ao**. (b) Through auxiliary winding **aa3**, (c) Extended winding **b1b3**. (d) Load voltage and current when $k_2 \geq 0$ and $k_1 = 0.5$.

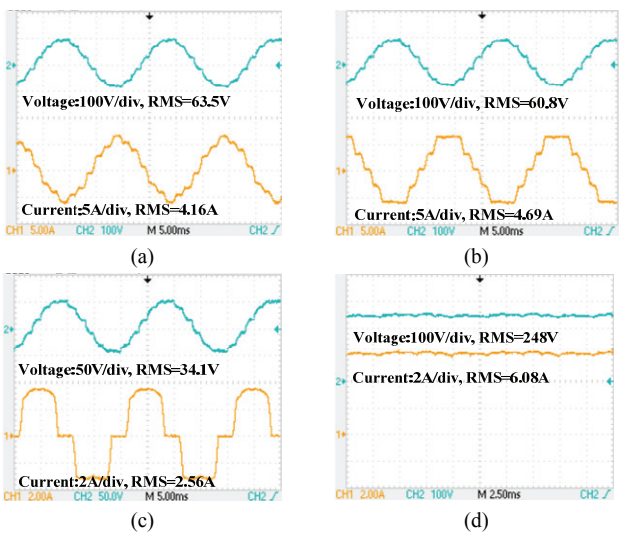

Fig. 17. Voltage and current. (a) Through the wye-connected winding **ao**. (b) Through auxiliary winding **a3a**, (c) Extended winding **b1b3**. (d) The load voltage and current when $k_2 \geq 0$ and $k_1 = 1$.

apparent power of the autotransformer is 211.6 VA, and the load power is 1011.8 W. Therefore, the equivalent kVA is 0.2091.

(3) $k_2 \geq 0$ and $k_1 = 0.5$: Fig. 16 shows the voltages across and current through the windings of core limb (a) and the load current and voltage when $k_2 \geq 0$ and $k_1 = 0.5$. The apparent power of the autotransformer is 502 VA, and the load power is 1029.6 W. Therefore, the equivalent kVA is 0.4876.

(4) $k_2 \geq 0$ and $k_1 = 1$: Fig. 17 shows the voltages across and current through the windings of core limb (a) and the load current and voltage when $k_2 \geq 0$ and $k_1 = 1$. The apparent power of the autotransformer is 723.9 VA, and the load power is 1085.9 W. Therefore, the equivalent kVA is 0.72.

(5) $k_2 \leq 0$ and $k_1 = -0.5$: Fig. 18 shows the voltages across and current through the windings of core limb (a) and the load current and voltage when $k_2 \leq 0$ and $k_1 = -0.5$. The apparent power of the autotransformer is 554.64 VA, and the load power is 959.76 W. Therefore, the equivalent kVA is 0.5779.

(6) $k_2 \leq 0$ and $k_1 = 0$: Fig. 19 shows the voltages across and current through the windings of core limb (a) and the load current and voltage when $k_2 \leq 0$ and $k_1 = 0$. The apparent power of the autotransformer is 388.8 VA, and the load power is 1458.4 W. Therefore, the equivalent

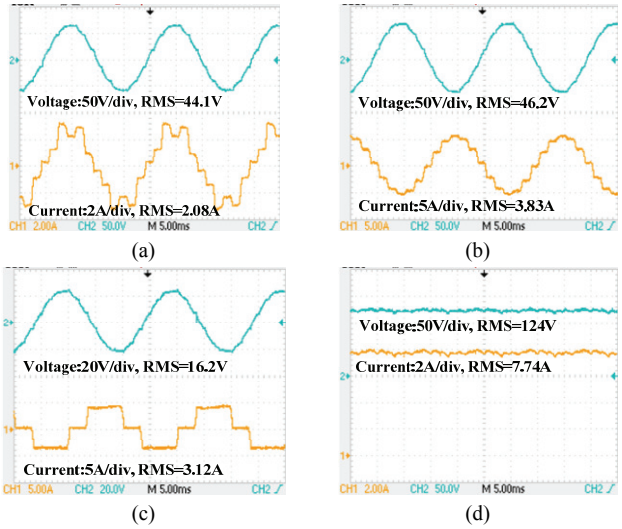

Fig. 18. Voltage and current. (a) Through the wye-connected winding **ao**, (b) Through auxiliary winding **aa3**. (c) Extended winding **b3b2**. (d) The load voltage and current when $k_2 \le 0$ and $k_1 = -0.5$.

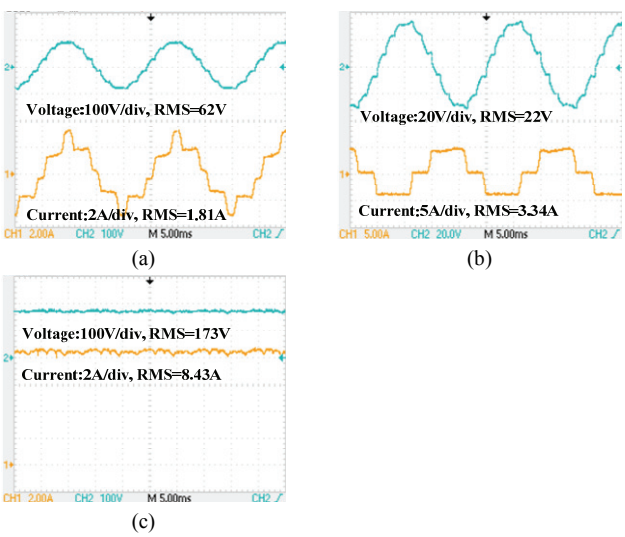

Fig. 19. Voltage and current. (a) Through the wye-connected winding **ao**. (b) Extended winding **b3b2**. (c) The load voltage and current when $k_2 \le 0$ and $k_1 = 0$.

kVA is 0.2666.

(7) $k_2 \le 0$ and $k_1 = 0.5$: Fig. 20 shows the voltages across and current through the windings of core limb (a) and the load current and voltage when $k_2 \le 0$ and $k_1 = 0.5$. The apparent power of the autotransformer is 763.91 VA, and the load power is 1447.4 W. Therefore, the equivalent kVA is 0.5278.

(8) $k_2 \le 0$ and $k_1 = 1$: Fig. 21 shows the voltages across and current through the windings of core limb (a) and the load current and voltage when $k_2 \le 0$ and $k_1 = 1$. The apparent power of the autotransformer is 1019 VA, and the load power is 1487.1 W. Therefore, the equivalent kVA is 0.6852.

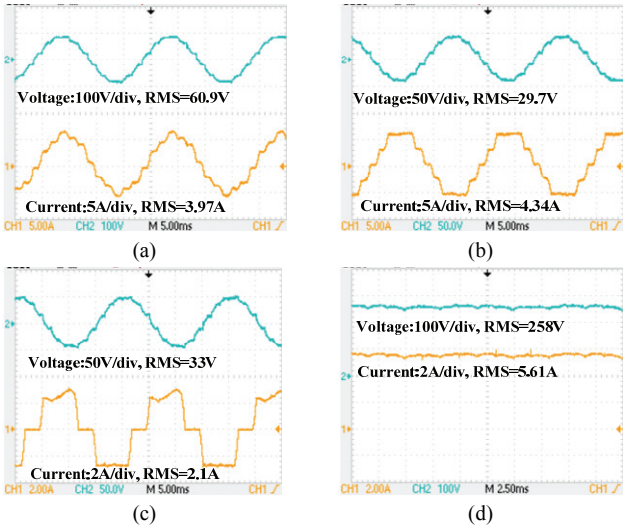

Fig. 20. Voltage and current. (a) Through the wye-connected winding **ao**. (b) Through auxiliary winding **aa3**. (c) Extended winding **b2b3**. (d) The load voltage and current when $k_2 \le 0$ and $k_1 = 0.5$.

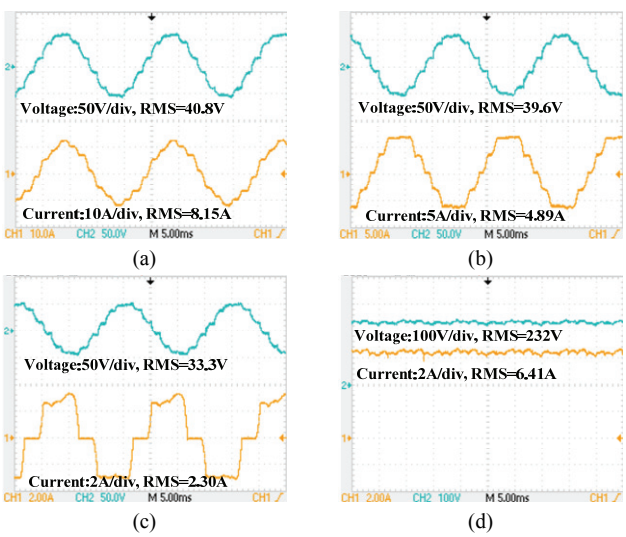

Fig. 21. Voltage and current. (a) Through the wye-connected winding **ao**, (b) Through auxiliary winding **aa3**. (c) Extended winding **b3b2**. (d) The load voltage and current when $k_2 \le 0$ and $k_1 = 1$.

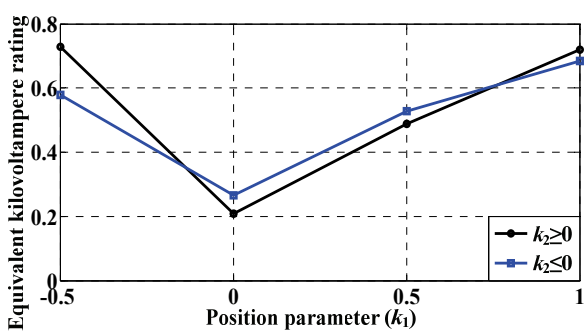

Fig. 22. Relation between the position and equivalent kVA rating under experiments.

Experimental results illustrate the relation between the position and equivalent kVA rating, as shown in Fig. 22. The equivalent kVA rating is minimal when $k_2 \geq 0$ and $k_1 = 0$, which is identical to the theoretical analysis.

Theoretical analysis and simulation results show that, when $k_2 \geq 0$ and $k_1 = 0$, the wye-connected autotransformer has the least equivalent kVA rating and the simplest winding configuration. When $k_2 \geq 0$ and $k_1 = 0$, the proportional parameter is $(2-\sqrt{3})$, and the turn ratio is equal to 0.8966.

VI. CONCLUSIONS

This study analyzes the effect of winding configuration on the kVA rating of a wye-connected autotransformer applied to a 12-pulse rectifier. Conclusions are obtained as follows:

(1) The position and proportional parameters are defined to describe the winding configuration of the wye-connected autotransformer. When the proportional parameter is greater than zero and the position parameter is equal to zero, the winding configuration of the wye-connected autotransformer is optimal. The optimal autotransformer has three windings on every core limb. When the autotransformer is applied to the 12-pulse rectifier, its equivalent kVA rating is approximately 21%.

(2) The winding configuration of the wye-connected autotransformer remarkably affects its equivalent kVA rating. Not all autotransformers of arbitrary winding configuration can reduce the equivalent kVA rating. The autotransformer has the least equivalent kVA rating and the simplest winding configuration only when it is optimally designed.

(3) The proposed method provides an interesting and useful confirmation that the well-designed autotransformer is optimal in terms of kVA rating. The method also offers an additional insight into these autotransformers and how they may be analyzed.

REFERENCES

[1] J. Solanki, N. Frohleke, J. Bocker, A. Averberg, and P. Wallmeier, "High-current variable-voltage rectifiers: state of the art topologies," *IET Power Electron.*, Vol. 8, No. 6, pp. 1068-1080, Jun. 2015.

[2] İ. Yilmaz, M. Ermis, and I. Cadirci, "Medium-frequency induction melting furnace as a load on the power system," *IEEE Trans. Ind. Appl.*, Vol. 48, No. 4, pp.1203-1214, May 2012.

[3] R. Fuentes, J. Estrada, L. Neira, and E. Barrientos, "Increasing copper production in electrochemical plants using new small transformer - rectifiers in parallel with existing power rectifiers," *IEEE_PCIC*, pp. 337-341, Nov. 2014.

[4] Z. Bing, K. J. Karimi, and J. Sun, "Input impedance modeling and analysis of line-commutated rectifiers," *IEEE Trans. Power Electron.*, Vol. 24, No. 10, pp. 2338-2346, Oct. 2009.

[5] F. Meng, L. Gao, S. Yang, and W. Yang, "Effect of phase-shift angle on a delta-connected autotransformer applied to a 12-pulse rectifier," *IEEE Trans. Ind. Electron.*, Vol. 62, No. 8, pp. 4678-4690, Aug. 2015.

[6] B. Singh, S. Gairola, B. N. Singh, A. Chandra, and K. AI-Haddad, "Multipulse AC-DC converters for improving power quality: a review," *IEEE Trans. Power Electron.*, Vol. 23, No. 1, pp. 260-281, Jan. 2008.

[7] R. Kalpana, G. Bhuvaneswari, B. Singh, S. Singh, and S. Gairola, "Autoconnected-transformer-based 20-pulse AC-DC converter for telecommunication power supply," *IEEE Trans. Ind. Electron.*, Vol. 60, No. 10, pp. 4178-4190, Oct. 2013.

[8] F. Meng, L. Gao, S. Yang, and W. Yang, "Effect of single-phasing on multipulse rectifier with active interphase reactor," *IEEE Trans. Power Electron.*, Vol. 30, No. 5, pp. 2549-2555, Jan. 2015.

[9] J. Solanki, N. Fröhleke, and J. Böcker, "Implementation of hybrid filter for 12-pulse thyristor rectifier supplying high-current variable-voltage DC load," *IEEE Trans. Ind. Electron.*, Vol. 62, No. 8, pp. 4691-4701, Aug. 2015.

[10] H. Akagi and K. Isozaki, "A hybrid active filter for a three-phase 12-pulse diode rectifier used as the front end of a medium-voltage motor drive," *IEEE Trans. Power Electron.*, Vol. 27, No. 1, pp. 69-77, Jan. 2012.

[11] F. Meng, W. Yang, and S. Yang, "Effect of voltage transformation ratio on the kilovoltampere rating of delta-connected autotransformer for 12-pulse rectifier system," *IEEE Trans. Ind. Electron.*, Vol. 60, No. 9, pp. 3579-3588, Jun. 2012.

[12] T. Yang, S. Bozhko, and G. Asher, "Functional modeling of symmetrical multipulse autotransformer rectifier units for aerospace applications," *IEEE Trans. Power Electron.*, Vol. 30, No. 9, pp. 4704-4713, Sep. 2015.

[13] M. M. Swamy, "An electronically isolated 12-pulse autotransformer rectification scheme to improve input power factor and lower harmonic distortion in variable frequency drives," *IEEE Trans. Ind. Appl.*, Vol. 51, No. 5, pp. 3986-3994, Sep./Oct. 2015.

[14] F. Meng, L. Gao, W. Yang, and S. Yang, "Comprehensive comparison of the delta- and wye-connected autotransformer applied to 12-pulse rectifier," *J. Modern Power Syst. Clean Energy*, Vol. 4, No. 1, pp. 135-145, Jan. 2016.

[15] D. A. Paice, *Power Electronic Converter Harmonics: Multipulse Methods for Clean Power*, USA: IEEE Press, 1996.

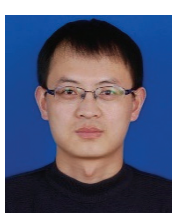

Fangang Meng was born in Shandong, China, in 1982. He received a B.S. degree in thermal energy and power engineering in 2005 and obtained M.S. and Ph.D. degrees in electrical engineering in 2007 and 2011, respectively, from the Harbin Institute of Technology, Harbin, China. Since 2011, he has been working as an assistant professor in the Harbin Institute of Technology at Weihai. His research interests include harmonic detection, stability analysis of converters, and high-power rectification.

Qingxiao Du was born in Shandong, China, in 1995. She received a B.S. degree in electrical engineering from the Harbin Institute of Technology, Weihai, China, in 2017 and an M.S. degree in electrical power engineering from the University of Southampton, Southampton, U.K., in 2018. Her current research interests include MPR and power electronic transformer.

Lei Gao was born in Hebei, China, in 1982. She received B.S., M.S., and Ph.D. degrees in electrical engineering from the Harbin Institute of Technology, Harbin, China, in 2005, 2007, and 2012, respectively. Since 2012, she has been working as an assistant professor in the Harbin Institute of Technology at Weihai. Her current research interests include power electronics and motor drives.

Quanhui Li was born in Shandong, China, in 1996. He received a B.S. degree in electrical engineering in 2018 from the Harbin Institute of Technology, Weihai, China. Since 2018, he has been working toward an M.S. degree in Power Electronics and Power Drives in the Harbin Institute of Technology at Weihai. His research interests include MPR and high-power rectification.

Zhongcheng Man was born in Shandong, China, in 1993. He received a B.S. degree in electrical engineering in 2017 from China University of Mining and Technology, Xuzhou, China. Since 2017, he has been working toward an M.S. degree in Power Electronics and Power Drives in the Harbin Institute of Technology at Weihai. His research interests include MPR, power electronic transformers, and high-power rectification.